ELSEVIER

SCIENCE DIRECT®

PHYSICS LETTERS B

Physics Letters B 554 (2003) 121–132

www.elsevier.com/locate/npe

Measuring the CP-violating phase by a long base-line neutrino experiment with Hyper-Kamiokande

Mayumi Aoki [a,b], Kaoru Hagiwara [a], Naotoshi Okamura [c]

[a] *Theory Group, KEK, Tsukuba, Ibaraki 305-0801, Japan*
[b] *Department of Physics, Ochanomizu University, Tokyo 112-8610, Japan*
[c] *IPPAP, Physics Department, Virginia Tech. Blacksburg, VA 24061, USA*

Received 28 August 2002; received in revised form 21 December 2002; accepted 25 December 2002

Editor: T. Yanagida

Abstract

We study the sensitivity of a long-base-line (LBL) experiment with neutrino beams from the High Intensity Proton Accelerator (HIPA), that delivers 10^{21} POT per year, and a proposed 1 Mt water Čerenkov detector, Hyper-Kamiokande (HK) 295 km away from the HIPA, to the CP phase ($\delta_{\rm MNS}$) of the three-flavor lepton mixing matrix. We examine a combination of the ν_μ narrow-band beam (NBB) at two different energies, $\langle p_\pi \rangle = 2$, 3 GeV, and the $\bar{\nu}_\mu$ NBB at $\langle p_\pi \rangle = 2$ GeV. By allocating one year each for the two ν_μ beams and four years for the $\bar{\nu}_\mu$ beam, we can efficiently measure the $\nu_\mu \to \nu_e$ and $\bar{\nu}_\mu \to \bar{\nu}_e$ transition probabilities, as well as the ν_μ and $\bar{\nu}_\mu$ survival probabilities. CP violation in the lepton sector can be established at 4σ (3σ) level if the MSW large-mixing-angle scenario of the solar-neutrino deficit is realized, $|\delta_{\rm MNS}|$ or $|\delta_{\rm MNS} - 180^\circ| > 30^\circ$, and if $4|U_{e3}|^2(1-|U_{e3}|^2) \equiv \sin^2 2\theta_{\rm RCT} > 0.03$ (0.01). The phase $\delta_{\rm MNS}$ is more difficult to constrain by this experiment if there is little CP violation, $\delta_{\rm MNS} \sim 0^\circ$ or 180°, which can be distinguished at 1σ level if $\sin^2 2\theta_{\rm RCT} \gtrsim 0.01$.

PACS: 14.60.Lm; 14.60.Pq; 01.50.My

Keywords: Neutrino oscillation experiment; Long base line experiments; Future plan

Neutrino oscillation experiment is one of the most attractive experiments in the first quarter of 21st century. Many experiments will measure precisely the model parameters in the neutrino oscillations. In this Letter, we discuss the sensitivity of a long-base-line (LBL) experiment with conventional neutrino beams to measure the CP phase in the lepton sector.

The Super-Kamiokande (SK) Collaboration showed that the ν_μ created in the atmosphere oscillates into ν_τ with almost maximal mixing [1]. The SNO Collaboration reported that the ν_e's from the sun oscillate into the other active neutrinos [2]. A consistent picture in the three active-neutrino framework is emerging.

In the three-neutrino-model, neutrino oscillations depend on two mass-squared differences, three mixing angles and one CP violating phase of the lepton-flavor mixing (Maki–Nakagawa–Sakata (MNS) [3]) matrix. These

E-mail addresses: mayumi.aoki@kek.jp (M. Aoki), nokamura@vt.edu (N. Okamura).

0370-2693/03
doi:10.1016/S0370-2693(02)03292-6

parameters are constrained by the solar and atmospheric neutrino observations. One of the mixing angles and one of the mass-squared differences are constrained by the atmospheric-neutrino observation, which we may label [4] as $\sin^2\theta_{\rm ATM}$ and $\delta m^2_{\rm ATM}$, respectively. The K2K experiment, the ongoing LBL neutrino oscillation experiment from KEK to SK, constrains the same parameters [5]. Their findings are consistent with the maximal mixing, $\sin^2 2\theta_{\rm ATM} \sim 1$ ($\sin^2\theta_{\rm ATM} \sim 0.5$) and $\delta m^2_{\rm ATM} \sim (2 \sim 4) \times 10^{-3}$ (eV^2). The solar-neutrino observations constrain another mixing angle and the other mass-squared difference, $\sin^2 2\theta_{\rm SOL}$ and $\delta m^2_{\rm SOL}$, respectively. Four possible solutions to the solar-neutrino deficit problem [6] are found: the MSW [7,8] large-mixing-angle (LMA) solution, the MSW small-mixing-angle (SMA) solution, the vacuum oscillation (VO) solution [9], and the MSW low-δm^2 (LOW) solution. The SK Collaboration [6] and the SNO Collaboration [2] suggested that the MSW LMA solution is the most favorable solution among them, for which $\sin^2 2\theta_{\rm SOL} = 0.7 \sim 0.9$ and $\delta m^2_{\rm SOL} = (3 \sim 15) \times 10^{-5}$ eV^2. For the third mixing angle, only the upper bound is obtained from the reactor neutrino experiments. CHOOZ [10] and Palo Verde [11] found $\sin^2 2\theta_{\rm RCT} < 0.1$ for $\delta m^2_{\rm ATM} \sim 3 \times 10^{-3}$ eV^2. No constraint on the CP phase ($\delta_{\rm MNS}$) has been reported.

Several future LBL neutrino-oscillation experiments [12–15] have been proposed to confirm the results of these experiments and to measure the neutrino oscillation parameters more precisely. One of those experiments proposed in Japan makes use of the beam from High Intensity Proton Accelerator (HIPA) [16] and SK as the detector [15]. The facility HIPA [16] has a 50 GeV proton accelerator to be completed by the year 2007 in the site of JAERI (Japan Atomic Energy Research Institute), as a joint project of KEK and JAERI. The proton beam of HIPA will deliver neutrino beams of sub-GeV to several GeV range, whose intensity will be two orders of magnitudes higher than that of the KEK PS beam for the K2K experiment. The HIPA-to-SK experiment with $L = 295$ km base-line length and $\langle E_\nu\rangle \simeq 1$ GeV will measure $\delta m^2_{\rm ATM}$ at about 3% accuracy and $\sin^2\theta_{\rm ATM}$ at about 1% accuracy from the ν_μ survival rate, while ν_μ-to-ν_e oscillation can be discovered if $\sin^2 2\theta_{\rm RCT} = 4|U^2_{e3}|(1 - |U^2_{e3}|) \gtrsim 0.006$ [15]. As a sequel to the HIPA-to-SK LBL experiment, prospects of using the HIPA beam for a very long base-line (VLBL) experiments with the base-line length of a few thousand km have been studied [4,17,18]. Use of narrow-band high-energy neutrino beams ($\langle E_\nu\rangle = 3 \sim 6$ GeV) and a 100 kt-level water Čerenkov detector [17] will allow us to distinguish the neutrino mass hierarchy (the sign of $m^2_3 - m^2_1$), if $\sin^2 2\theta_{\rm RCT} \gtrsim 0.03$ [4]. If the LMA solution of the solar neutrino deficit is chosen by the nature, we can further constrain the allowed region of the $\delta_{\rm MNS}$ and $\sin^2 2\theta_{\rm RCT}$ [4]. However, because $\bar\nu_\mu \to \bar\nu_e$ appearance is strongly suppressed by the matter effect at such high energies, the measurement is not sensitive to the CP violating effects, $\sim \sin\delta_{\rm MNS}$. In this Letter, we study the capability of an LBL experiment between HIPA and Hyper-Kamiokande (HK), a megaton-level water Čerenkov detector being proposed to be built at the Kamioka site [19]. Here a combination of the shorter distance ($L = 295$ km) and low ν-energy ($\langle E_\nu\rangle \sim 1$ GeV) makes the matter effect small, and the comparison of $\nu_\mu \to \nu_e$ and $\bar\nu_\mu \to \bar\nu_e$ appearance experiments is expected to have sensitivity to the CP violation effects proportional to $\sin\delta_{\rm MNS}$.

The MNS matrix of the three-neutrino model is defined as

$$\nu_\alpha = \sum_{i=1}^{3} (V_{\rm MNS})_{\alpha i}\,\nu_i = \sum_{i=1}^{3} (U_{\rm MNS})_{\alpha i}\,\mathcal{P}_{ii}\,\nu_i, \tag{1}$$

where $\alpha = e, \mu, \tau$ are the lepton-flavor indices and ν_i $(i = 1, 2, 3)$ denotes the neutrino mass-eigenstates. The 3×3 MNS matrix, $V_{\rm MNS}$, has three mixing angles and three phases in general for Majorana neutrinos. In the above parameterization, the two Majorana phases reside in the diagonal phase matrix $\mathcal{P}$, and the matrix U, which has three mixing angles and one phase, can be parameterized in the same way as the CKM matrix [20]. Because the present neutrino oscillation experiments constrain directly the elements, U_{e2}, U_{e3} and $U_{\mu 3}$, we find it most convenient to adopt the parameterization [21] where these three matrix elements in the upper-right corner of the U matrix are chosen as the independent parameters. Without losing generality, we can take U_{e2} and $U_{\mu 3}$ to be real and non-negative while U_{e3} is a complex number. All the other matrix elements of the U are then determined by the unitary conditions [21].

The probability of finding the flavor-eigenstate β at base-line length L in the vacuum from the original flavor-eigenstate α is given by

$$P_{\nu_\alpha\to\nu_\beta} = \left|U_{\beta1}U^*_{\alpha2} + U_{\beta2}e^{-i\Delta_{12}}U^*_{\alpha2} + U_{\beta3}e^{-i\Delta_{13}}U^*_{\alpha3}\right|^2, \tag{2}$$

where

$$\Delta_{ij} \equiv \frac{m_j^2 - m_i^2}{2E_\nu}L \simeq 2.534\frac{\delta m^2_{ij}\ (\mathrm{eV}^2)}{E_\nu\ (\mathrm{GeV})}L\ (\mathrm{km}) \tag{3}$$

satisfy $\Delta_{12} + \Delta_{23} + \Delta_{31} = (\delta m^2_{12} + \delta m^2_{23} + \delta m^2_{31})(L/2E_\nu) = 0$. The two independent mass-squared differences are identified with the two "measured" ones, as follows:

$$\delta m^2_{\mathrm{SOL}} = \left|\delta m^2_{12}\right| \ll \left|\delta m^2_{13}\right| = \delta m^2_{\mathrm{ATM}}. \tag{4}$$

With the above identification, the MNS matrix elements are constrained by the observed survival probabilities, $P_{\nu_\mu\to\nu_\mu}$ from the atmospheric neutrinos [22], $P_{\bar\nu_e\to\bar\nu_e}$ from the reactor antineutrinos [10,11], and $P_{\nu_e\to\nu_e}$ from the solar neutrinos [6]. The four independent parameters of the MNS matrix are then related to the observed oscillation amplitudes as

$$|U_{e3}|^2 = \left(1 - \sqrt{1 - \sin^2 2\theta_{\mathrm{RCT}}}\right)/2, \tag{5a}$$

$$(U_{\mu3})^2 \equiv \sin^2\theta_{\mathrm{ATM}} = \left(1 \pm \sqrt{1 - \sin^2 2\theta_{\mathrm{ATM}}}\right)/2, \tag{5b}$$

$$\left(U^2_{e2}\right)^2 = \left(1 - |U_{e3}|^2 - \sqrt{\left(1 - |U_{e3}|^2\right)^2 - \sin^2 2\theta_{\mathrm{SOL}}}\right)/2, \tag{5c}$$

$$\arg(U_{e3}) = -\delta_{\mathrm{MNS}}. \tag{5d}$$

The CP phase of the MNS matrix, δ_{MNS}, is not constrained. The solution Eq. (5c) follows from our convention [4], $U_{e1} > U_{e2}$, which defines the mass-eigenstate ν_1. In this convention, there are four mass hierarchy cases corresponding to the sign of δm^2_{ij}; I ($\delta m^2_{13} > \delta m^2_{12} > 0$), II ($\delta m^2_{13} > 0 > \delta m^2_{12}$), III ($\delta m^2_{12} > 0 > \delta m^2_{13}$), and IV ($0 > \delta m^2_{12} > \delta m^2_{13}$) [4]. If the MSW effect is relevant for the solar neutrino oscillation, then the neutrino mass hierarchy cases II and IV are not favored. When $\sin^2 2\theta_{\mathrm{ATM}} \neq 1$, there is an additional twofold ambiguity in the determination of $U_{\mu3}$ in Eq. (5b). In order to avoid the ambiguity, we adopt the $U_{\mu3}$ element itself, or equivalently $\sin^2\theta_{\mathrm{ATM}}$ defined in Eq. (5b), as an independent parameter of the MNS matrix. Summing up, we parametrize the three-flavor neutrino oscillation parameters in terms of the 5 observed (constrained) parameters $\delta m^2_{\mathrm{ATM}}$, $\delta m^2_{\mathrm{SOL}}$, $\sin^2\theta_{\mathrm{ATM}}$, $\sin^2 2\theta_{\mathrm{SOL}}$, $\sin^2 2\theta_{\mathrm{RCT}}$ and one CP-violating phase δ_{MNS}, for four hierarchy cases.

Neutrino-flavor oscillation inside of the matter is governed by the Schrödinger equation

$$i\frac{\partial}{\partial t}\begin{pmatrix}\nu_e\\ \nu_\mu\\ \nu_\tau\end{pmatrix} = H\begin{pmatrix}\nu_e\\ \nu_\mu\\ \nu_\tau\end{pmatrix} = \frac{1}{2E_\nu}\left[H_0 + \begin{pmatrix}a & 0 & 0\\ 0 & 0 & 0\\ 0 & 0 & 0\end{pmatrix}\right]\begin{pmatrix}\nu_e\\ \nu_\mu\\ \nu_\tau\end{pmatrix}, \tag{6}$$

where H_0 is the Hamiltonian in the vacuum and a is the matter effect term [7]

$$a = 2\sqrt{2}\,G_F n_e E_\nu = 7.56\times10^{-5}\ (\mathrm{eV}^2)\left(\frac{\rho}{\mathrm{g/cm}^3}\right)\left(\frac{E_\nu}{\mathrm{GeV}}\right). \tag{7}$$

Here n_e is the electron density of the matter, E_ν is the neutrino energy, G_F is the Fermi constant, and ρ is the matter density. In our analysis, we assume for brevity that the density of the earth's crust relevant for the LBL experiment, between HIPA and HK is a constant, $\rho = 3$, with an overall uncertainty of $\Delta\rho = 0.1$;

$$\rho\left(\mathrm{g/cm}^3\right) = 3.0 \pm 0.1. \tag{8}$$

The Hamiltonian is diagonalized as

$$H = \frac{1}{2E_\nu}\widetilde{U}\begin{pmatrix}\lambda_1 & 0 & 0\\ 0 & \lambda_2 & 0\\ 0 & 0 & \lambda_3\end{pmatrix}\widetilde{U}^\dagger, \tag{9}$$

by the MNS matrix in the matter $\widetilde{U}$. The neutrino-flavor oscillation probabilities in the matter

$$P_{\nu_\alpha\to\nu_\beta} = \left|\widetilde{U}_{\beta1}\widetilde{U}^*_{\alpha1} + \widetilde{U}_{\beta2}e^{-i\tilde{\Delta}_{12}}\widetilde{U}^*_{\alpha2} + \widetilde{U}_{\beta3}e^{-i\tilde{\Delta}_{13}}\widetilde{U}^*_{\alpha3}\right|^2, \tag{10}$$

takes the same form as those in the vacuum, with $\tilde{\Delta}_{ij} = (\lambda_j - \lambda_i)L/2E_\nu$, if the matter density can be approximated by a constant throughout the base-line. Because the effective matter potential for antineutrinos has the opposite sign with the same magnitude, the total Hamiltonian $\overline{H}$ governing the antineutrino oscillation in the matter is obtained from H as follows [4],

$$\overline{H}\left(\delta m^2_{12}, \delta m^2_{13}\right) = -H^*\left(-\delta m^2_{12}, -\delta m^2_{13}\right). \tag{11}$$

We make the following simple treatments in estimating the signals and the backgrounds in our analysis.

- We assume a 1 Mt water Čerenkov detector, which is capable of distinguishing between $e^\pm$ CC events and $\mu^\pm$ CC events, but cannot distinguish their charges.
- We do not require capability of the detector to reconstruct the neutrino energy.

Although the water Čerenkov detector has the capability of measuring the energy of the produced μ and e as well as a part of hadronic activities, we do not make use of these information in this analysis. We only use the total numbers of the produced $\mu^\pm$ and $e^\pm$ events from ν_μ or $\bar{\nu}_\mu$ narrow-band-beams (NBB). The NBBs from HIPA deliver 10^{21} protons on target (POT) in a typical 1 yr operation, corresponding to about 100 days of operation with the design intensity [16]. Details of the NBBs used for this study are available from the web-page [23].

In the following discussion, we examine ν_μ NBBs with the mean π momentum $\langle p_\pi\rangle = 2$ GeV (NBB(2 GeV)) and $\langle p_\pi\rangle = 3$ GeV (NBB(3 GeV)), and $\bar{\nu}_\mu$ NBB with $\langle p_\pi\rangle = 2$ GeV ($\overline{\text{NBB}}$(2 GeV)). For our input ('true') value of $\delta m^2_{\text{ATM}} = 3.5\times10^{-3}$ eV^2, the probability $P_{\nu_\mu\to\nu_e}$ has a broad peak at $E_\nu \sim 1$ GeV. NBB(2 GeV) and $\overline{\text{NBB}}$(2 GeV) are chosen to maximize the transition probability, since $\langle E_\nu\rangle \simeq \langle p_\pi\rangle/2$. Because $P_{\nu_\mu\to\nu_e}$ does not change much in the range $E_\nu \simeq 0.6 \sim 1.2$ GeV, our results do not depend strongly on the true value of the δm^2_{ATM}: as long as it stays in the range $(2\sim5)\times10^{-3}$ eV^2 [4].

The signals in this analysis are the numbers of ν_μ and ν_e CC events from NBB(2, 3 GeV) and those of the $\bar{\nu}_\mu$ and $\bar{\nu}_e$ CC events from $\overline{\text{NBB}}$(2 GeV). These are calculated as

$$N_\ell\left(\nu_\mu;\langle p_\pi\rangle\right) = MN_A\int_0^{10\,\text{GeV}} dE_\nu\,\Phi_{\nu_\mu}\left(E_\nu;\langle p_\pi\rangle\right)P_{\nu_\mu\to\nu_\ell}(E_\nu)\sigma^{\text{CC}}_{\nu_\ell}(E_\nu), \tag{12a}$$

$$\overline{N}_{\bar{\ell}}\left(\bar{\nu}_\mu;\langle p_\pi\rangle\right) = MN_A\int_0^{10\,\text{GeV}} dE_{\bar{\nu}}\,\overline{\Phi}_{\bar{\nu}_\mu}\left(E_{\bar{\nu}};\langle p_\pi\rangle\right)P_{\bar{\nu}_\mu\to\bar{\nu}_\ell}(E_{\bar{\nu}})\sigma^{\text{CC}}_{\bar{\nu}_\ell}(E_{\bar{\nu}}), \tag{12b}$$

for $\ell = e$ or μ, where M is the mass of detector (1 Mt), $N_A = 6.017\times10^{23}$ is the Avogadro number, $\Phi_{\nu_\mu}(E_\nu;\langle p_\pi\rangle)$ and $\overline{\Phi}_{\bar{\nu}_\mu}(E_{\bar{\nu}};\langle p_\pi\rangle)$ are the flux of ν_μ in NBB($\langle p_\pi\rangle$ GeV) and $\bar{\nu}_\mu$ in $\overline{\text{NBB}}$($\langle p_\pi\rangle$ GeV), respectively. The flux is negligibly small at $E_\nu > 10$ GeV for the NBBs used in our analysis. The cross sections are obtained by assuming a pure water target [24].

Table 1
Expected number of CC signal events from $\nu_\mu \to \nu_\mu, \nu_e$ oscillations for NBB(2 GeV), NBB(3 GeV) and those from $\bar{\nu}_\mu \to \bar{\nu}_\mu, \bar{\nu}_e$ oscillations for $\overline{\text{NBB}}$ (2 GeV), with 1 Mt yr exposure. The results are shown for the parameters of Eqs. (13)

$\sin^2 2\theta_{\text{RCT}}$	δ_{MNS}	NBB ($\langle p_\pi \rangle = 2$ GeV)		NBB ($\langle p_\pi \rangle = 3$ GeV)		$\overline{\text{NBB}}$ ($\langle p_\pi \rangle = 2$ GeV)	
		N_μ	N_e	N_μ	N_e	$\overline{N}_{\bar{\mu}}$	$\overline{N}_{\bar{e}}$
0.06	0°	5.0×10^3	8.5×10^2	1.6×10^4	1.1×10^3	1.6×10^3	2.2×10^2
	90°	5.1×10^3	5.9×10^2	1.6×10^4	8.0×10^2	1.6×10^3	2.8×10^2
	180°	5.1×10^3	7.9×10^2	1.6×10^4	9.1×10^2	1.6×10^3	2.0×10^2
	270°	5.1×10^3	1.1×10^3	1.6×10^4	1.2×10^3	1.6×10^3	1.5×10^2
0.01	0°	5.1×10^3	1.7×10^2	1.6×10^4	2.3×10^2	1.6×10^3	4.5×10^1
	90°	5.1×10^3	6.2×10^1	1.6×10^4	9.5×10^1	1.6×10^3	6.7×10^1
	180°	5.1×10^3	1.4×10^2	1.6×10^4	1.4×10^2	1.6×10^3	3.7×10^1
	270°	5.1×10^3	2.5×10^2	1.6×10^4	2.7×10^2	1.6×10^3	1.6×10^1

Typical numbers of expected CC signals are tabulated in Table 1 for the parameter sets:[1]

$$\sin^2\theta_{\text{ATM}} = 0.5, \qquad \delta m^2_{13} = \delta m^2_{\text{ATM}} = 3.5\times10^{-3}\ \text{eV}^2, \tag{13a}$$

$$\sin^2 2\theta_{\text{SOL}} = 0.8, \qquad \delta m^2_{12} = \delta m^2_{\text{SOL}} = 1.0\times10^{-4}\ \text{eV}^2, \tag{13b}$$

$$\sin^2 2\theta_{\text{RCT}} = 0.06,\ 0.01, \qquad \delta_{\text{MNS}} = 0^\circ,\ 90^\circ,\ 180^\circ,\ 270^\circ, \tag{13c}$$

$$\rho = 3\ \text{g/cm}^3. \tag{13d}$$

The numbers in the Table 1 are for 1 Mt yr exposure with 10^{21} POT per year for 0.77 MW operation of HIPA at $L = 295$ km. From Table 1, we learn that the transition events, N_e and $\overline{N}_{\bar{e}}$, are sufficiently large to have the potential of distinguishing the CP conserved cases, $\delta_{\text{MNS}} = 0^\circ$ and 180°, from the CP violating cases of $\delta_{\text{MNS}} = 90^\circ$ and 270°, even if $\sin^2 2\theta_{\text{RCT}} = 0.01$. We also find that the survival events, N_μ and $\overline{N}_{\bar{\mu}}$, barely depend on the CP phase. The ratio $\overline{N}_{\bar{\mu}}(2\text{ GeV})/N_\mu(2\text{ GeV})$ is approximately $\sigma^{\text{CC}}_{\nu_\mu}/\sigma^{\text{CC}}_{\bar{\nu}_\mu} \simeq 2.9$, because both the flux and the survival rates are approximately the same for ν_μ and $\bar{\nu}_\mu$ [4]. From the comparison of $N_\ell(2\text{ GeV})$ and $N_\ell(3\text{ GeV})$, we find that $N_\mu(3\text{ GeV})/N_\mu(2\text{ GeV}) \sim 3$ because of the rise in the cross section (∼1.5) and the increase in the survival rate (∼2). The ν_e appearance signal N_e increases only slightly at higher energies because a slight decrease in the transition probability cancels partially the effect of the rising cross section. Most notably, we find that the difference between the predictions of $\delta_{\text{MNS}} = 0^\circ$ and 180° cases is significantly larger for $N_e(\nu_\mu; \langle p_\pi \rangle = 3\text{ GeV})$ than that for $N_e(\nu_\mu; \langle p_\pi \rangle = 2\text{ GeV})$.

The above results can be seen clearly in Fig. 1, where we show the expected number of $\bar{\nu}_e$ CC events $\overline{N}_{\bar{e}}$ for $\overline{\text{NBB}}$(2 GeV) with 4 Mt yr plotted against those of the ν_e CC event N_e for NBB(2 GeV) (left) and for NBB(3 GeV) (right), both with 1 Mt yr. The CP-phase dependence of the predictions are shown as closed circles for the parameters of Eqs. (13) at $\sin^2 2\theta_{\text{RCT}} = 0.06$, 0.04, 0.02 and 0.01. Comparable numbers of $\bar{\nu}_e$ CC events ($\overline{N}_{\bar{e}}$) and ν_e CC events (N_e) are expected by giving 4 times more $\bar{\nu}_\mu$ than ν_μ beams. At each $\sin^2 2\theta_{\text{RCT}}$ the $\nu_\mu \to \nu_e$ events are expected to be smaller at $\delta_{\text{MNS}} = 90^\circ$ (solid squares) than at $\delta_{\text{MNS}} = 270^\circ$ (open squares). The trend is opposite for the $\bar{\nu}_\mu \to \bar{\nu}_e$ events, and thus anticorrelation allows us to distinguish the two cases clearly. On the other hand, the expected number at $\delta_{\text{MNS}} = 0^\circ$(solid circles) and that at $\delta_{\text{MNS}} = 180^\circ$(open circles) do not differ much for NBB(2 GeV) and $\overline{\text{NBB}}$ 2 GeV. We find that NBB(3 GeV) predicts significant differences between the two CP-invariant cases without loosing event numbers.

[1] Recently KamLAND Collaboration confirmed that only the LMA solution of the solar-neutrino deficit problem is consistent with the data [26]. The allowed region of δm^2_{SOL} is found to be either (6–9) or (13–19) $\times 10^{-5}$ eV^2, slightly below or above our input value. The conclusions of this Letter remain valid no matter which region its true value is.

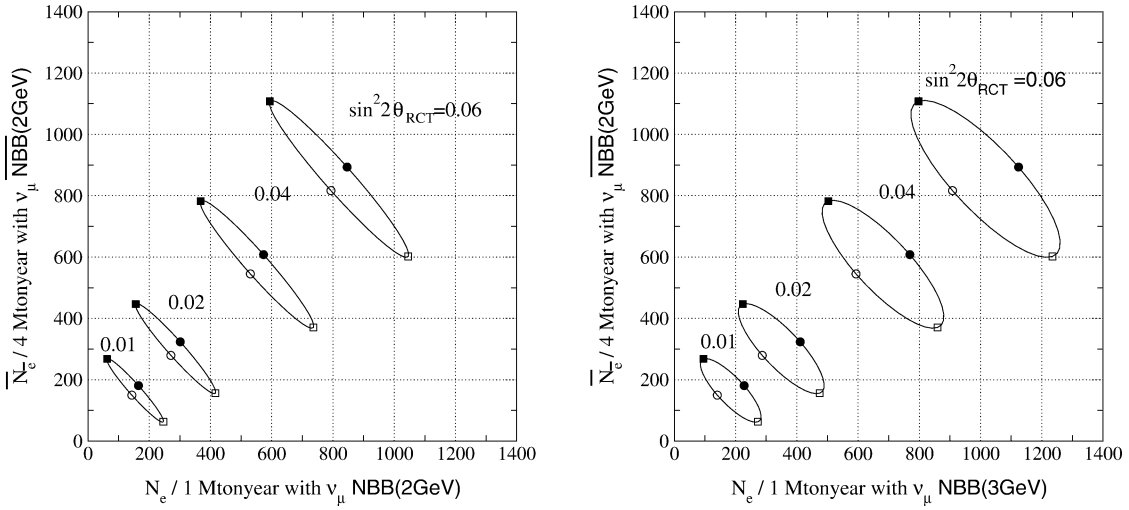

Fig. 1. The CP phase dependence of $N_{\bar{e}}(\bar{\nu}_\mu; 2\text{ GeV})$ for 4 Mt yr plotted against $\overline{N}_e(\nu_\mu; 2\text{ GeV})$ for 1 Mt yr in the left figure, and against $N_e(\nu_\mu; 3\text{ GeV})$ for 1 Mt yr in the right figure. $\delta_{\text{MNS}} = 0°$ (solid circle), $\delta_{\text{MNS}} = 90°$ (solid square), $\delta_{\text{MNS}} = 180°$ (open circle), and $\delta_{\text{MNS}} = 270°$ (open square). The results are for the parameters at Eqs. (13).

In this Letter, we assume 1 Mt yr exposure each with NBB(2 GeV) and NBB(3 GeV) and 4 Mt yr exposure of $\overline{\text{NBB}}$(2 GeV), and examine the capability of HIPA-to-Hyper-Kamiokande experiments to measure the CP phase, δ_{MNS}, under the following simplified treatments of the backgrounds and systematic errors.

For the ν_e and ν_μ CC signal from NBB(ν_μ; $\langle p_\pi \rangle$), $N_e(\nu_\mu; \langle p_\pi \rangle)$ and $N_\mu(\nu_\mu; \langle p_\pi \rangle)$, respectively, we consider the following backgrounds:

$$N_e\big(\langle p_\pi \rangle\big)_{\text{BG}} = N_e\big(\nu_e; \langle p_\pi \rangle\big) + N_{\bar{e}}\big(\bar{\nu}_\mu; \langle p_\pi \rangle\big) + N_{\bar{e}}\big(\bar{\nu}_e; \langle p_\pi \rangle\big) + N_{e,\bar{e}}\big(\text{NC}; \langle p_\pi \rangle\big), \tag{14a}$$

$$N_\mu\big(\langle p_\pi \rangle\big)_{\text{BG}} = N_\mu\big(\nu_e; \langle p_\pi \rangle\big) + N_{\bar{\mu}}\big(\bar{\nu}_\mu; \langle p_\pi \rangle\big) + N_{\bar{\mu}}\big(\bar{\nu}_e; \langle p_\pi \rangle\big). \tag{14b}$$

The first 3 terms in the r.h.s. are calculated as

$$N_{\substack{(-)\\ \ell}}\big(\overset{(-)}{\nu}_\alpha; \langle p_\pi \rangle\big) = MN_A \int_0^{10\text{ GeV}} dE_\nu\, \Phi_{\substack{(-)\\ \nu_\alpha}}\big(E_\nu; \langle p_\pi \rangle\big) P_{\substack{(-)\\ \nu_\alpha \to \nu_\ell}}(E_\nu) \sigma^{\text{CC}}_{\substack{(-)\\ \nu_\ell}}(E_\nu), \tag{15}$$

where Φ_{ν_α} and $\Phi_{\bar{\nu}_\alpha}$ stands, respectively, for the secondary ν_α and $\bar{\nu}_\alpha$ flux of the primarily ν_μ NBB. The last term in Eq. (14a) for the e-like events gives the contribution of the NC events where produced π^0's mimic the electron shower in the HK. By using the estimations from the K2K experiments [5], we use

$$N_{e,\bar{e}}\big(\text{NC}; \langle p_\pi \rangle\big) = P_{e/\text{NC}} \sum_{\nu_\alpha = \nu_e, \bar{\nu}_e, \nu_\mu, \bar{\nu}_\mu} N^{\text{NC}}_{\nu_\alpha}\big(\langle p_\pi \rangle\big), \tag{16}$$

with

$$P_{e/\text{NC}} = 0.25 \times (1 \pm 0.1)\%, \tag{17}$$

where the NC event numbers are calculated as in Eq. (15) by replacing $\sigma^{\text{CC}}_{\nu_\ell}$ by $\sigma^{\text{NC}}_{\nu_\ell}$. The 10% error in the misidentification probability of 0.25% is accounted for as a systematic error [15]. The τ-lepton contribution is found to be negligibly small for the NBBs considered in this analysis. The background for the $\bar{\nu}_\mu$ enriched beam $\overline{\text{NBB}}$(2 GeV) are evaluated in the same way.

Table 2
Expected number of the CC and NC events at HK in the absence of oscillations. The results are for 1 Mt yr for the ν_μ enriched NBBs and 4 Mt yr for $\bar{\nu}_\mu$ enriched NBB from HIPA. The numbers in the parenthesis give the fraction of each mode against the main mode whose numbers are shown in boldface

NBB($\langle p_\pi \rangle$)		ν_μ	ν_e	$\bar{\nu}_\mu$	$\bar{\nu}_e$
NBB(2 GeV)	CC	$\mathbf{2.8 \times 10^4}(1)$	$2.2 \times 10^2(0.008)$	$1.9 \times 10^2(0.007)$	$1.3 \times 10^1(0.0005)$
1 Mt yr	NC	$\mathbf{1.1 \times 10^4}(1)$	$8.1 \times 10^1(0.007)$	$8.1 \times 10^1(0.007)$	5.3(0.0004)
NBB(3 GeV)	CC	$\mathbf{4.5 \times 10^4}(1)$	$3.1 \times 10^2(0.007)$	$2.0 \times 10^2(0.004)$	$1.5 \times 10^1(0.0003)$
1 Mt yr	NC	$\mathbf{1.6 \times 10^4}(1)$	$1.1 \times 10^2(0.006)$	$8.6 \times 10^1(0.005)$	6.3(0.0004)
$\overline{\text{NBB}}$(2 GeV)	CC	$3.0 \times 10^3(0.09)$	$1.9 \times 10^2(0.005)$	$\mathbf{3.5 \times 10^4}(1)$	$2.5 \times 10^2(0.007)$
4 Mt yr	NC	$1.2 \times 10^3(0.08)$	$6.9 \times 10^1(0.005)$	$\mathbf{1.5 \times 10^4}(1)$	$1.0 \times 10^2(0.007)$

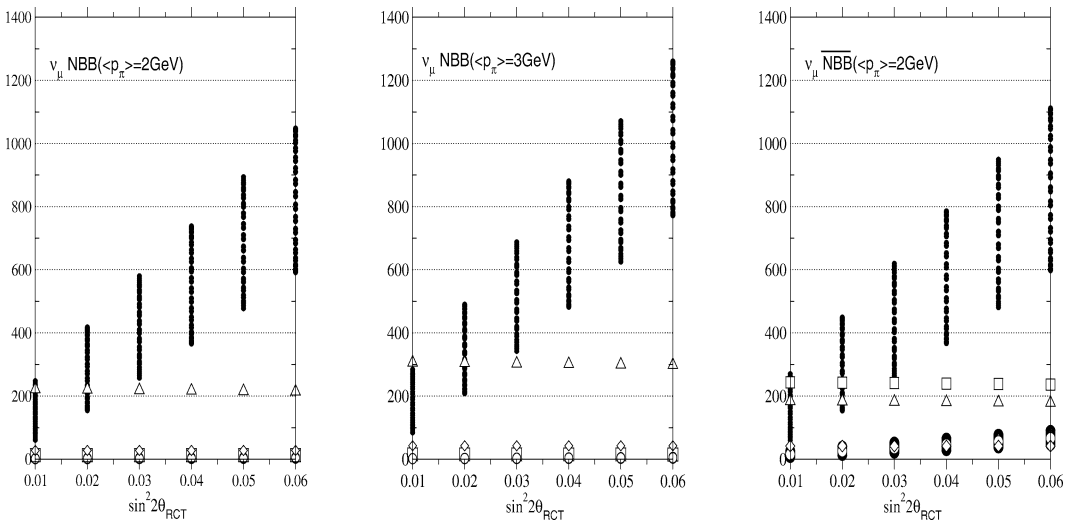

Fig. 2. The $\sin^2 2\theta_{\text{RCT}}$ dependence of the expected signal and background event numbers for the parameters of Eqs. (13) for $\sin^2 2\theta_{\text{RCT}} = 0.01 \sim 0.06$. Solid circles stand for the number of expected signal events for $\delta_{\text{MNS}} = n \times 10^\circ$ ($n = 1 \sim 36$). Open diamonds denote the π^0 background from the NC events. Open triangles and open square show ν_e and $\bar{\nu}_e$ survival events. Open circles are $\bar{\nu}_\mu \to \bar{\nu}_e$ transition events for $\overline{\text{NBB}}$(2, 3 GeV) and $\nu_\mu \to \nu_e$ transition events for $\overline{\text{NBB}}$(2 GeV).

Summing up, the event numbers for each energy neutrino and antineutrino NBBs are calculated from the sum:

$$N_\ell\big(\langle p_\pi \rangle\big) = N_\ell\big(\nu_\mu; \langle p_\pi \rangle\big) + N_\ell\big(\langle p_\pi \rangle\big)_{\text{BG}}, \tag{18a}$$

$$\overline{N}_\ell\big(\langle p_\pi \rangle\big) = \overline{N}_{\bar{\ell}}\big(\bar{\nu}_\mu; \langle p_\pi \rangle\big) + \overline{N}_\ell\big(\langle p_\pi \rangle\big)_{\text{BG}}. \tag{18b}$$

Most importantly, we do not require the capability of the HK detector to distinguish charges of electrons and muons. In Table 2 the expected numbers of CC and NC events at HK in the absence of oscillations are shown for 1 Mt yr each for the ν_μ enriched NBBs and 4 Mt yr for $\bar{\nu}_\mu$ enriched NBB. The event numbers from the main (enriched) neutrinos are shown in boldface. The numbers in the parenthesis are the fractions as compared to the corresponding main mode. From the comparison between NBB(2 GeV) and $\overline{\text{NBB}}$(2 GeV), we find that the fraction of the secondary-beam contributions is much larger for the $\bar{\nu}_\mu$-beam than that for the ν_μ-beam. This is essentially because $\bar{\nu}_\ell$ CC cross section is about a factor of three smaller than the ν_ℓ CC cross section at $E_\nu \sim 1$ GeV.

In Fig. 2, we show the expected $\nu_\mu \to \nu_e$ ($\bar{\nu}_\mu \to \bar{\nu}_e$) signal and background event numbers for the parameters of Eqs. (13) for $\sin^2 2\theta_{\text{RCT}} = 0.01 \sim 0.06$. The solid circles show the number of expected signal events for

$\delta_{\rm MNS} = n \times 10^\circ$ ($n = 1 \sim 36$). The numbers of signal events are largest at around $\delta_{\rm MNS} = 270^\circ$ for NBB(2, 3 GeV), while those for $\overline{\rm NBB}$(2 GeV) are largest at around 90°, as is expected from the CP phase dependence of N_e and $\overline{N}_{\bar{e}}$ shown in Fig. 1. The open triangle denotes $\nu_e \to \nu_e$ CC events, which give the largest background for the experiments with NBB(2, 3 GeV), and the second largest background for $\overline{\rm NBB}$(2 GeV). The open square denotes $\bar{\nu}_e \to \bar{\nu}_e$ CC events that gives the largest background for $\overline{\rm NBB}$(2 GeV), but is negligible for NBB(2, 3 GeV). The open diamond denotes the background from the NC events, where π^0's are miss-identified as electrons. They give the second largest background for NBB(2, 3 GeV). Backgrounds from $\bar{\nu}_\mu \to \bar{\nu}_e$ transition events for NBB(2, 3 GeV) and those from $\nu_\mu \to \nu_e$ transition events for $\overline{\rm NBB}$(2 GeV) are shown by open circle. These transition backgrounds depend on the CP phase and they tend to cancel the $\delta_{\rm MNS}$ dependence of the signals, but their magnitudes are small. The background level starts dominating the signal at $\sin^2 2\theta_{\rm RCT} \lesssim 0.02$.

The background numbers for the μ-like signals are found to be negligibly small ($\sim 10^{-2}$) for $\overline{\rm NBB}$(2, 3 GeV). Those for $\overline{\rm NBB}$(2 GeV) are found to be about 21% of the signal almost independent of $\sin^2 2\theta_{\rm RCT}$. In both cases, the major background comes from the secondary $\bar{\nu}_\mu$ (ν_μ) survival events.

Our analysis proceeds as follows. For a given set of the model parameters, we calculate the expected numbers of all the signal and background events for each NBB($\langle p_\pi \rangle$) and $\overline{\rm NBB}$($\langle p_\pi \rangle$), by assuming 100% detection efficiencies for simplicity. The resulting numbers of μ-like and e-like events are then denoted by $N_\mu^{\rm true}(\langle p_\pi \rangle)$ and $N_e^{\rm true}(\langle p_\pi \rangle)$ for NBB($\langle p_\pi \rangle$), and $\overline{N}_\mu^{\rm true}(\langle p_\pi \rangle)$ and $\overline{N}_e^{\rm true}(\langle p_\pi \rangle)$ for $\overline{\rm NBB}$($\langle p_\pi \rangle$).

We account for the following two effects as major parts of the systematic uncertainty in this analysis. One is the uncertainty in the total flux of each neutrino beam, for which we assign the uncertainty,

$$\overset{(-)}{f}_{\nu_\alpha}\big(\langle p_\pi \rangle\big) = 1 \pm 0.03, \tag{19}$$

independently for $\nu_\alpha = \nu_e, \nu_\mu, \bar{\nu}_e, \bar{\nu}_\mu$ and for NBB(2 GeV), NBB(3 GeV), and $\overline{\rm NBB}$(2 GeV). Although it is likely that correlation exists among the flux uncertainties, we ignore possible effects of correlations in this analysis. By using the above flux factors, theoretical predictions for the event numbers, $N_\ell^{\rm fit}(\langle p_\pi \rangle)$ and $\overline{N}_\ell^{\rm fit}(\langle p_\pi \rangle)$, are calculated as

$$\begin{aligned} N_\ell^{\rm fit}\big(\langle p_\pi \rangle\big) &= f_{\nu_e}\big(\langle p_\pi \rangle\big) N_\ell\big(\nu_e, \langle p_\pi \rangle\big) + f_{\nu_\mu}\big(\langle p_\pi \rangle\big) N_\ell\big(\nu_\mu, \langle p_\pi \rangle\big) + f_{\bar{\nu}_e}\big(\langle p_\pi \rangle\big) N_{\bar{\ell}}\big(\bar{\nu}_e, \langle p_\pi \rangle\big) \\ &\quad + f_{\bar{\nu}_\mu}\big(\langle p_\pi \rangle\big) N_{\bar{\ell}}\big(\bar{\nu}_\mu, \langle p_\pi \rangle\big) + \delta_{\ell,e} P_{e/\rm NC} \sum_{\nu_\alpha} f_{\nu_\alpha}\big(\langle p_\pi \rangle\big) N_{\nu_\alpha}^{\rm NC}\big(\langle p_\pi \rangle\big), \end{aligned} \tag{20a}$$

$$\begin{aligned} \overline{N}_\ell^{\rm fit}\big(\langle p_\pi \rangle\big) &= \bar{f}_{\nu_e}\big(\langle p_\pi \rangle\big) \overline{N}_\ell\big(\nu_e, \langle p_\pi \rangle\big) + \bar{f}_{\nu_\mu}\big(\langle p_\pi \rangle\big) \overline{N}_\ell\big(\nu_\mu, \langle p_\pi \rangle\big) + \bar{f}_{\bar{\nu}_e}\big(\langle p_\pi \rangle\big) \overline{N}_{\bar{\ell}}\big(\bar{\nu}_e, \langle p_\pi \rangle\big) \\ &\quad + \bar{f}_{\bar{\nu}_\mu}\big(\langle p_\pi \rangle\big) \overline{N}_{\bar{\ell}}\big(\bar{\nu}_\mu, \langle p_\pi \rangle\big) + \delta_{\ell,e} P_{e/\rm NC} \sum_{\nu_\alpha} \bar{f}_{\nu_\alpha}\big(\langle p_\pi \rangle\big) \overline{N}_{\nu_\alpha}^{\rm NC}\big(\langle p_\pi \rangle\big), \end{aligned} \tag{20b}$$

where the last terms proportional to $\delta_{\ell,e}$ are counted only for $\ell = e$. As the second major systematic error, we allocate 3.3% overall uncertainty in the matter density along the base-line, Eq. (8). The fit functions are hence calculated for an arbitrary set of the 6 model parameters, the 12 flux normalization factors, and the matter density ρ.

The χ^2 function of the fit in this analysis can now be expressed as

$$\begin{aligned} \chi^2 &= \sum_{\rm NBB} \left\{ \left(\frac{N_\mu^{\rm fit}(\langle p_\pi \rangle) - N_\mu^{\rm true}(\langle p_\pi \rangle)}{\sigma_\mu(\langle p_\pi \rangle)} \right)^2 + \left(\frac{N_e^{\rm fit}(\langle p_\pi \rangle) - N_e^{\rm true}(\langle p_\pi \rangle)}{\sigma_e(\langle p_\pi \rangle)} \right)^2 + \sum_{\nu_\alpha} \left(\frac{f_{\nu_\alpha}(\langle p_\pi \rangle) - 1.0}{0.03} \right)^2 \right\} \\ &\quad + \sum_{\overline{\rm NBB}} \left\{ \left(\frac{\overline{N}_\mu^{\rm fit}(\langle p_\pi \rangle) - \overline{N}_\mu^{\rm true}(\langle p_\pi \rangle)}{\sigma_\mu(\langle p_\pi \rangle)} \right)^2 + \left(\frac{\overline{N}_e^{\rm fit}(\langle p_\pi \rangle) - \overline{N}_e^{\rm true}(\langle p_\pi \rangle)}{\sigma_e(\langle p_\pi \rangle)} \right)^2 + \sum_{\nu_\alpha} \left(\frac{\bar{f}_{\nu_\alpha}(\langle p_\pi \rangle) - 1.0}{0.03} \right)^2 \right\} \\ &\quad + \left(\frac{\rho - 3.0}{0.1} \right)^2 + \left(\frac{\delta m^{2\,\rm fit}_{\rm SOL} - \delta m^{2\,\rm true}_{\rm SOL}}{0.1 \times \delta m^{2\,\rm true}_{\rm SOL}} \right)^2 + \left(\frac{\sin^2 2\theta^{\rm fit}_{\rm SOL} - \sin^2 2\theta^{\rm true}_{\rm SOL}}{0.06} \right)^2, \end{aligned} \tag{21}$$

where the summation is over NBB(2 GeV), NBB(3 GeV) and $\overline{\text{NBB}}$(2 GeV). Even though we have only one $\overline{\text{NBB}}$ in our analysis, we retain the summation symbol in Eq. (21) for the sake of clarity. The last two terms are added because KamLAND experiment [25] will measure δm^2_{SOL} at 10% level and the solar neutrino experiments constrain $\sin^2 2\theta_{\text{SOL}}$ with the 1σ error of about 0.06 for the LMA parameters of Eqs. (13). The individual error for each $N_\mu(\langle p_\pi\rangle)$ ($\overline{N}_\mu(\langle p_\pi\rangle)$) is statistical only, whereas the error for each $N_e(\langle p_\pi\rangle)$ ($\overline{N}_e(\langle p_\pi\rangle)$) is a sum of the statistical errors and the systematic error coming from the 10% uncertainty in the e/π^0 misidentification probability of Eq. (17),

$$\sigma_\mu\big(\langle p_\pi\rangle\big) = \sqrt{N_\mu^{\text{true}}\big(\langle p_\pi\rangle\big)}, \tag{22a}$$

$$\sigma_e\big(\langle p_\pi\rangle\big) = \sqrt{N_e^{\text{true}}\big(\langle p_\pi\rangle\big) + \big(0.1 N_{e,\bar{e}}^{\text{true}}(\text{NC};\langle p_\pi\rangle)\big)^2}. \tag{22b}$$

The errors for the $\overline{\text{NBB}}$(2 GeV) case are calculated similarly as above.

We show in Fig. 3 regions allowed by the HIPA-to-HK experiment in the plain of $\sin^2 2\theta_{\text{RCT}}$ and δ_{MNS}. The mean values of the input data are calculated for the LMA parameters of Eqs. (13). In each figure, the input parameter point ($\sin^2 2\theta_{\text{RCT}}^{\text{true}}$, $\delta_{\text{MNS}}^{\text{true}}$) is shown by a solid circle for $\sin^2 2\theta_{\text{RCT}}^{\text{true}} = 0.06$, and by a solid square for $\sin^2 2\theta_{\text{RCT}}^{\text{true}} = 0.01$. The regions where $\chi^2_{\text{min}} < 1$, 4, and 9 are depicted by solid, dashed, and dotted boundaries, respectively. All the 6 parameters, $\delta m^{2\,\text{fit}}_{\text{ATM}}$, $\sin^2\theta^{\text{fit}}_{\text{ATM}}$, $\delta m^{2\,\text{fit}}_{\text{SOL}}$, $\sin^2 2\theta^{\text{fit}}_{\text{SOL}}$ $\sin^2 2\theta^{\text{fit}}_{\text{RCT}}$, $\delta^{\text{fit}}_{\text{MNS}}$, the matter density ρ^{fit}, and the 12 flux normalization factors are allowed to vary freely in the fit.

From the top-right and bottom-right figures for $\delta_{\text{MNS}}^{\text{true}} = 90^\circ$ and 270°, respectively, we learn that δ_{MNS} can be constrained to $\pm 30^\circ(\pm 60^\circ)$ at the 1σ (3σ) level, even if $\sin^2 2\theta_{\text{RCT}}^{\text{true}} = 0.01$. This is because $N_e + \overline{N}_e$ constrain $\sin^2 2\theta_{\text{RCT}}$ and $N_e/\overline{N}_e$ distinguishes between $\delta_{\text{MNS}} = 90^\circ$ and 270° in Fig. 3, whereas the remaining parameters (δm^2_{ATM} and $\sin^2\theta_{\text{ATM}}$) are constrained by the ν_μ and $\bar{\nu}_\mu$ survival data, N_μ and $\overline{N}_\mu$. The accuracy of the δ_{MNS} measurement does not decrease significantly for $\sin^2 2\theta_{\text{RCT}}^{\text{true}} = 0.01$ despite the large background level, because the δ_{MNS}-dependence of the signal exceeds significantly the 3% uncertainty of the background level from the flux normalization factors in Eq. (19). We find that the CP violation signal can be distinguished from the CP-conserving cases ($\delta_{\text{MNS}} = 0^\circ$ or 180°) at 4σ (3σ) level for all δ_{MNS} values in the region $|\delta_{\text{MNS}}|$, $|\delta_{\text{MNS}} - 180^\circ| > 30^\circ$ if $\sin^2 2\theta_{\text{RCT}}^{\text{true}} \gtrsim 0.03$ (0.01), for the LMA parameters of Eqs. (13) and for the systematic errors assumed in this analysis.

The situation is quite different for the CP-conserving cases of $\delta_{\text{MNS}}^{\text{true}} = 0^\circ$ or 180° shown in the left-hand side of Fig. 3. δ_{MNS} can be constrained to better than $\pm 7^\circ(11^\circ)$ accuracy at 1σ level for $\sin^2 2\theta_{\text{RCT}} \gtrsim 0.06$ (0.01), but the two cases cannot be distinguished at 2σ level. This is mainly because of the similarity of $N_e/\overline{N}_e$ between $\delta_{\text{MNS}} = 0^\circ$ and 180° in Fig. 1. The difference between the two cases is larger for NBB(3 GeV). If we remove the NBB(3 GeV) data from the fit, we find that the two cases cannot be distinguished even at 1σ level. This two-fold ambiguity between δ_{MNS} and $180^\circ - \delta_{\text{MNS}}$ is found in general for all δ_{MNS}, because the difference in the predictions can be adjusted by a shift in the fitted $\sin^2 2\theta_{\text{RCT}}$ value; see Fig. 1.

As a demonstration of the effect of using two NBBs, NBB(2 GeV) and NBB(3 GeV), in the analysis, we show in Fig. 4 the fit results when the data are generated by using NBB(2 GeV) and $\overline{\text{NBB}}$(2 GeV) only, each at 2 Mt yr and 4 Mt yr, respectively. It is clearly seen from the figures that the 'mirror' solution at $\delta_{\text{MNS}} = 180^\circ$ (0°) can fit the data as well as the 'true' solution at $\delta_{\text{MNS}} = 0^\circ$ (180°). Essentially the same results are obtained when we replace NBB(2 GeV) by NBB(3 GeV) in the above analysis. It is only by combining the two NBBs that we can distinguish the two solutions as shown in Fig. 3. We find less significant difference from the results of Fig. 3 when the input δ_{MNS} value is 90° or 270°.

It is remarkable that the 1σ error of δ_{MNS} is as large as 30° for $\delta_{\text{MNS}}^{\text{true}} = 90^\circ$ and 270° while it is less than 10° for $\delta_{\text{MNS}}^{\text{true}} = 0^\circ$ and 180°. This is simply because the δ_{MNS} dependence of the ν_μ-to-ν_e (and also $\bar{\nu}_\mu$-to-$\bar{\nu}_e$) oscillation probability is roughly proportional to $\sin\delta_{\text{MNS}}$, in the vicinity of the first dip of the ν_μ-to-ν_μ survival probability.

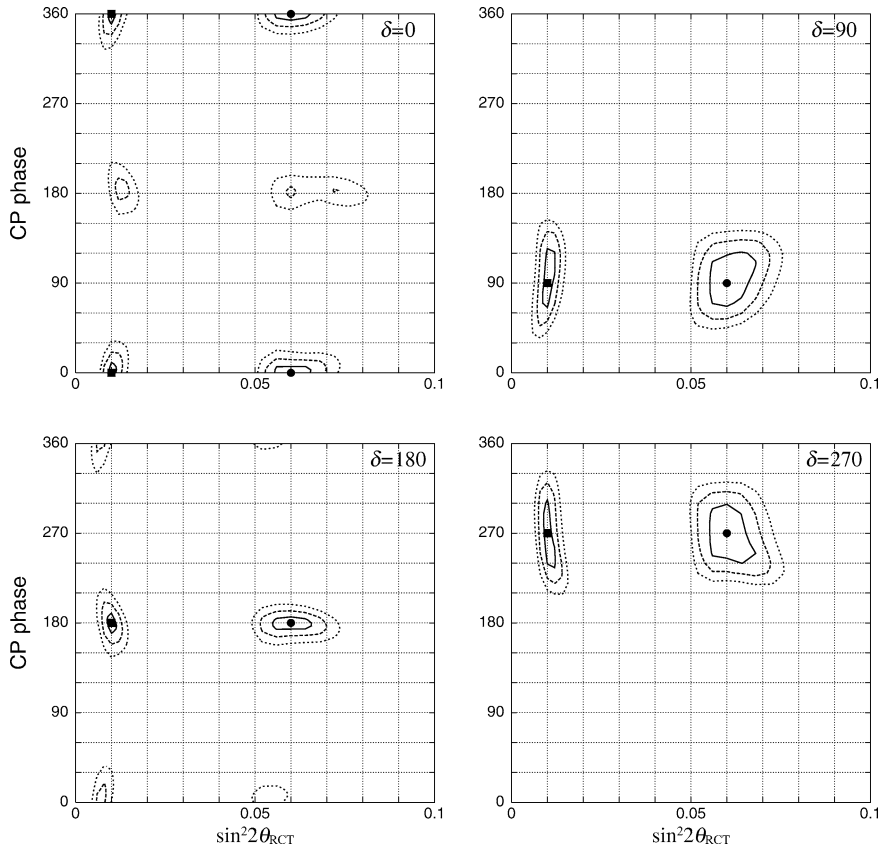

Fig. 3. Regions allowed by the HIPA-to-HK experiment are shown in the plain of $\sin^2 2\theta_{\mathrm{RCT}}$ and δ_{MNS}. The assumed experimental conditions are 1 Mt yr each for NBB(2 GeV) and NBB(3 GeV), and 4 Mt yr for $\overline{\mathrm{NBB}}$(2 GeV) with 10^{21} POT/yr. The input data are calculated for the LMA parameters of Eqs. (13). In each figure, the input parameter point ($\sin^2 2\theta^{\mathrm{true}}_{\mathrm{RCT}}, \delta^{\mathrm{true}}_{\mathrm{MNS}}$) is shown by a solid circle for $\sin^2 2\theta^{\mathrm{true}}_{\mathrm{RCT}} = 0.06$, and by a solid square for $\sin^2 2\theta^{\mathrm{true}}_{\mathrm{RCT}} = 0.01$. The regions where $\chi^2_{\mathrm{min}} < 1$, 4, and 9 are depicted by solid, dashed, and dotted boundaries, respectively.

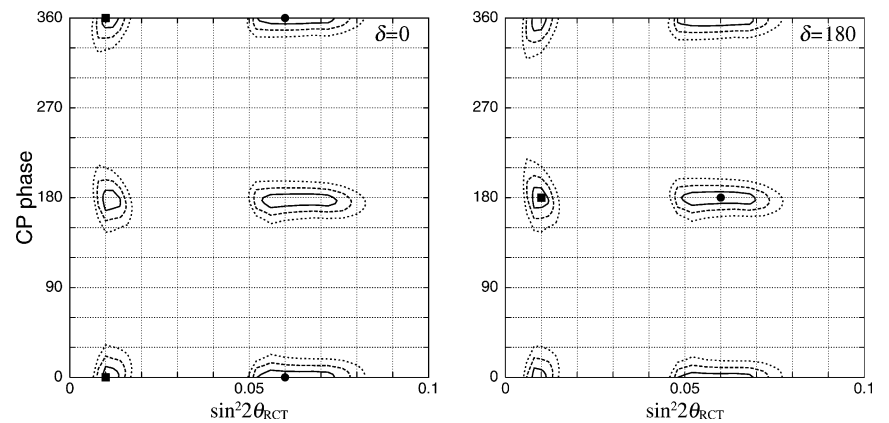

Fig. 4. The same as Fig. 3 but with 2 Mt yr for NBB(2 GeV) and 4 Mt yr for $\overline{\mathrm{NBB}}$(3 GeV) only. The two-fold ambiguity in the fit is clearly seen.

We close this Letter by pointing out that the low-energy LBL experiment like HIPA-to-HK cannot distinguish between the neutrino-mass hierarchy cases (between I and III) because of the small matter effect at low energies. If we repeat the analysis by using the same input data but assuming the hierarchy III in the analysis, we obtain another excellent fit to all the data where the fitted model parameters are slightly shifted from their true (input) values. VLBL experiments at higher energies at $L > 1000$ km [4] are needed to determine the mass hierarchy.

Acknowledgements

The authors wish to thank stimulating discussions with T. Kajita, T. Kobayashi and J. Sato. The work of M.A. is supported in part by the Grant-in-Aid for Scientific Research from MEXT, Japan. K.H. would like to thank the core-university program of JSPS for support. The work of N.O. is supported in part by a grand from the US Department of Energy, DE-FG05-92ER40709.

References

[1] Super-Kamiokande Collaboration, Phys. Rev. Lett. 85 (2000) 3999;
And see also Super-Kamiokande Collaboration's home page, http://www-sk.icrr.u-tokyo.ac.jp/.
[2] SNO Collaboration, Phys. Rev. Lett. 89 (2002) 011301;
SNO Collaboration, Phys. Rev. Lett. 89 (2002) 011302;
And see also SNO Collaboration's home page, http://www.sno.phy.queensu.ca/.
[3] Z. Maki, M. Nakagawa, S. Sakata, Prog. Theor. Phys. 28 (1962) 870.
[4] M. Aoki, et al., hep-ph/0112338;
M. Aoki, et al., hep-ph/0104220;
M. Aoki, hep-ph/0204008;
N. Okamura, hep-ph/0204118.
[5] K. Nishikawa, Presented at the XXth Int. Conf. on Neutrino Physics and Astrophysics, Munich, May 2002, http://neutrino2002.ph.tum.de/;
See also K2K experiment home page, http://neutrino.kek.jp/index.html.
[6] M. Smy, Presented at the XXth Int. Conf. on Neutrino Physics and Astrophysics, Munich, May 2002;
T. Kirsten, Presented at the XXth Int. Conf. on Neutrino Physics and Astrophysics, Munich, May 2002;
K. Lande, Presented at the XXth Int. Conf. on Neutrino Physics and Astrophysics, Munich, May 2002;
P. de Holanda, A. Smirnov, Presented at the XXth Int. Conf. on Neutrino Physics and Astrophysics, Munich, May 2002.
[7] L. Wolfenstein, Phys. Rev. D 17 (1978) 2369.
[8] S.P. Mikheyev, A.Yu. Smirnov, Yad. Fiz. 42 (1985) 1441, Sov. J. Nucl. Phys. 42 (1986) 913;
S.P. Mikheyev, A.Yu. Smirnov, Nuovo Cimento C 9 (1986) 17.
[9] B. Pontecorvo, Zh. Eksp. Teor. Fiz. 53 (1967) 1717;
S.M. Bilenky, B. Pontecorvo, Phys. Rep. 41 (1978) 225;
V. Barger, R.J.N. Phillips, K. Whisnant, Phys. Rev. D 24 (1981) 538;
S.L. Glashow, L.M. Krauss, Phys. Lett. B 190 (1987) 199.
[10] CHOOZ Collaboration, Phys. Lett. B 420 (1998) 397.
[11] F. Boehm, et al., Phys. Rev. Lett. 84 (2000) 3764;
F. Boehm, et al., Phys. Rev. D 62 (2000) 072002;
F. Boehm, et al., Phys. Rev. D 64 (2001) 112001.
[12] See MINOS Collaboration's home page, http://www-numi.fnal.gov:8875/.
[13] ICARUS Collaboration, hep-ex/0103008;
See also ICARUS Collaboration's home page, http://www.aquila.infn.it/icarus/.
[14] A. Rubbia, Nucl. Phys. Proc. Suppl. 91 (2000) 223;
See also OPERA Collaboration's home page, http://operaweb.web.cern.ch/operaweb/index.shtml.
[15] JHF Neutrino Working Group, hep-ex/0106019;
See also JHF Neutrino Working Group's home page, http://neutrino.kek.jp/jhfnu/.
[16] See HIPA's home page, http://jkj.tokai.jaeri.go.jp/.
[17] H. Chen, et al., hep-ph/0104266;
Y.F. Wang, et al., Phys. Rev. D 65 (2002) 073021.

[18] P. Huber, M. Lindner, W. Winter, Nucl. Phys. B 645 (2002) 3.
[19] E.g., T. Nakaya, Presented at the XXth Int. Conf. on Neutrino Physics and Astrophysics, Munich, May 2002.
[20] N. Cabibbo, Phys. Rev. Lett. 10 (1964) 531;
M. Kobayashi, T. Maskawa, Prog. Theor. Phys. 49 (1973) 652.
[21] K. Hagiwara, N. Okamura, Nucl. Phys. B 548 (1999) 60.
[22] M. Shiozawa, Presented at the XXth Int. Conf. on Neutrino Physics and Astrophysics, Munich, May 2002.
[23] See the home page, http://neutrino.kek.jp/~kobayasi/50gev/beam/0101.tables.
[24] See, e.g., K. Ishihara, Ph.D. Thesis, ICRR-Report-457-2000-1;
Y. Hayato, Talk at NuInt01, KEK, December 13–16, to appear in the proceedings.
[25] P. Alivisatos, et al., Proposal of the KamLAND experiment RCNS-98-15, STANFORD-HEP-98-03, July 1998, pp. 121;
K. Inoue, Presented at First Sendai International Conference on Neutrino Science, Sendai, Japan, March 2002, http://www.awa.tohoku.ac.jp/conf2002/;
See also KamLAND Collaboration's home page, http://www.awa.tohoku.ac.jp/html/KamLAND/index.html.
[26] KamLAND Collaboration, hep-ex/0212021.